# A molecular model to explain the controlled release from SBA-15 functionalized with APTES

Antonio L. Doadrio,[1] José M. Sanchez-Montero,[2] Juan C. Doadrio,[1] Antonio J. Salinas,[1,3] María Vallet-Regí[1,3*]

[1] *Departamento de Química Inorgánica y Bioinorgánica. Facultad de Farmacia. Universidad Complutense. 28040 Madrid. Spain. Instituto de Investigación I+12, Hospital 12 de Octubre. Madrid. Spain.*

[2] *Departamento de Química Orgánica y Farmacéutica. UCM. 28040. Madrid. Spain*

[3] *Centro de Investigación Biomédica en Red de Bioingeniería, Biomateriales y Nanomedicina, CIBER-BBN, Spain.*

*Corresponding Author:

Phone +34-913941861.

Fax +34-913941786.

E-mail: vallet@ucm.es

## A B S T R A C T

A molecular model with the approximate pore diameter of SBA-15 was constructed for the first time to investigate the effect of functionalize the matrix with 3-aminopropyl-triethoxy-silane (APTES) in the release of Chicago Sky Blue 6B (CSB). It was expected that the positively charged amino groups of APTES could interact with the negatively charged sulphonic groups of CSB allowing controlling the release process. Indeed the experimental study showed that the release kinetics of CSB from SBA-15-APTES is two orders of magnitude smaller than from native SBA-15. However molecular modelling calculations investigating the possible interactions of APTES and SBA-15 yield unexpected results. In the model including only the condensation between the silanol groups of SBA-15 and APTES, the calculated interaction energy of CSB was quite similar than with the model of native SBA-15. However when additional electrostatic interactions of the $-NH_2$ groups of APTES with the mesoporous matrix were modelled the mesoporous channels underwent a considerable deformation. These results point to the structure deformation as the cause of the greater retention of CSB in SBA-15-APTES and warn about the special features of APTES when used to functionalize mesoporous silica materials. The model built in this paper could be used to construct predictive models in analogous drug delivery systems.



**KEYWORDS:** Molecular modelling; Mesoporous SBA-15; APTES functionalisation; Chicago Sky Blue 6B; Kinetics of release.

## 1. Introduction

Molecular modelling is revealing as an important tool to understand the interactions between a drug and a material surface for its possible use in therapeutics [1-6]. In this context, mesoporous silica matrixes are receiving great attention for the controlled release of drugs in blood plasma [7-10]. These materials developed and characterized at the 90s of past century [11-15] were proposed in the past decade as matrixes for drug delivery systems [16,17]. Contrary to crystalline silica, silica particles without a long range, as SBA-15, are not toxic and commonly are used, as a colloid, in food additives and vitamin supplements. Further, silica has a surface enriched with OH, i.e. has a hydrophilic surface that is suitable to increase the circulation time in biological systems, for instance blood. Other materials have also been used in controlled release, such as hydrotalcite in human fibroblasts. Recently has been encountered a new application relative as inhibitor of macrophage migration inhibitory factor [18,19]. On the other hand, the kinetics of release of different drugs from mesoporous matrixes was established [20]. Aspects related with the mechanisms justifying the different retention of the drug after functionalizing the mesoporous matrixes remain unclear. In this sense molecular modelling could help to understand the experimental data and to establish the mechanism why the matrix functionalization modifies the kinetics of release.

In a previous study a molecular model of a mesoporous matrix functionalized with non-polar chains allowed to justify the kinetic results in an unexpected way. The theoretical model showed that the release process was fundamentally governed by the electrostatic drug-matrix interactions [21]. In the present work, models with the approximate dimensions of SBA-15 before and after be functionalized with the polar molecule 3-aminopropyl-triethoxy-silane (APTES) were constructed for the first time to investigate the Chicago Sky Blue-6B (CSB) release from both matrixes. APTES contains positively charged amino groups able to interact with the negatively charged sulphonic groups of CSB. Model drug CSB is a colorant which biological actions starting to be described including the inhibition of L-glutamate uptake into synaptic vesicles [22,23], anti-HIV capability [24,25] or the inhibition of $Ca^{2+}$ calmodulin-dependent protein kinase phosphatase [26]. The possible interactions of APTES and the SBA-15 mesoporous matrix as well as of CSB with SBA-15 and SBA-15-APTES were modelling. The theoretical results are compared with the experimental data of release to obtain a mechanism that explains the variations in the kinetics of release observed after functionalizing the matrix. The final aim of the methodology here presented is to use the molecular modelling as a tool to build predictive models in the development of new drug delivery systems from mesoporous matrixes.

## 2. Experimental section

### *2.1. Synthesis and chemical modification of SBA-15 mesoporous materials*

SBA-15 synthesis was made by using block copolymer surfactants in very acid solutions following the method reported by Zhao *et al.* [27] 41 g of triblock copolymer Pluronic® P123 [poly (ethylene glycol)-block-poly (propylene glycol)-block-poly (ethylene glycol), Mav =5800, Sigma-Aldrich] were dissolved in 138 g of D. I. water and 12.2 g of HCl 37 wt% (Sigma-Aldrich) at 40 ºC. After 1 h, 8.2 g of tetraethyl orthosilicate (TEOS, Sigma-Aldrich) were added. After aging under continuous stirring at 100 ºC for 24 h in a closed Teflon® recipient, the solid product was collected by filtration in glass plate and dried overnight in air at 40 ºC. The surfactant was removed by calcination; by increasing the temperature from room temperature to 550 ºC under nitrogen flow over 2 h, followed by 3 h heating at the same temperature in air.

A second material was obtained by modifying the pore walls of SBA-15 by the functionalization with APTES (Sigma-Aldrich). 200 mg of SBA-15 were kept under inert atmosphere (Argon) for 1 h and then refluxed with 0.08 mL of APTES in 20 mL of acetonitrile Sigma-Aldrich), during 24 h, under continuous stirring. The final samples were cooled, filtered and washed with acetonitrile and methanol and dried at 60 ºC for 24 h to obtain SBA-15 modified material, identified as SBA15-APTES.

*2.2. Loading and releasing of Chicago Sky Blue*

Powders of SBA–15 and SBA15–APTES materials were loaded by soaking in a solution of CSB prepared by dissolving 100 mg of CSB in 20 ml of methanol for 72 h at room temperature with constant stirring. The solid:drug weight ratio was 1:1. CSB molecule, 6,6'-[(3,3-dimethoxy[1,1'-biphenyl]-4,4'-dyil) bis(azo)] bis[4-amino-4-hydroxy-1,3-napthalenedisulphonic acid] tetrasodium salt, was supplied by Tocris distributor Biogen Cientifica. The final samples were filtered, rinsed with methanol, and dried overnight at 30 ºC. The release profile of CSB was obtained by soaking the samples in 40 mL of a simulated body fluid solution (SBF) [28] buffered at physiological pH of 7.4 at 37 ºC, with continuous stirring at 200 r.p.m.

*2.3. Characterization*

Samples were characterized by X-ray diffraction, XRD, using a Philips X'Pert MDP (Cu Kα radiation) diffractometer, Fourier Transform Infrared Spectroscopy, FTIR, with a Nicolet Nexus spectrometer equipped with a diamond ATR Golden Gate accessory and $N_2$ adsorption, in a Micrometrics ASAP 2010 porosimeter. Before the $N_2$ adsorption measurements, the samples were outgassed 24 h at 60 ºC. Pore diameter was calculated using a geometric relation between pore volume obtained by the Barrett-

Joyner-Halenda, BJH, method [29] and the spacing of the $d_{10}$ reflection obtained by low angle XRD, for 2D-hexagonal mesopores structure [30].

The percentage of functionalization of SBA15–APTES was measured by elemental analysis in a Perkin Elmer 2400 CHN analyzer. On the other hand, the amount of CSB adsorbed in the mesoporous matrixes was quantified by Elemental Analysis in a Macroanalyser LECO CHNS-932 and Thermogravimetric Analysis, TGA, carried out between 25 and 1200 ºC in oxygen atmosphere (flow rate 100 mL/min; heating rate 10 ºC/min) using a Perking Elmer TG/TDA instrument.

A Reversed Phase High Performance Liquid Chromatography (RP-HPLC) in a Waters Alliance 2695 separation module (Milford, Massachusetts, USA) based on a mobile phase of 30% methanol-70% water (v/v) at a flow rate of 1 mL/min was used to quantify the CSB release. The system was equipped with a variable-wavelength diode array detector Waters 2996 and controlled by Millenium 32 software, at 240 nm and 45 ºC oven temperature. An X-Terra RP-18 reversed-phase column (5 μm, 150 x 4.6 mm), supplied by Waters, was employed. The injection volume was 10 μL and the retention time 2 min.

*2.4. Molecular modelling calculations*

A model analogous to the 3D hexagonal structure of SBA-15 was built modifying a MCM-41 layer model obtained elsewhere [12,31]. An accepted structure for these materials consists of hexagonal arrays of variable length embedded in a matrix of amorphous silica. This structure is modelled by stacking the pseudo cell, $Si_6O_{18}$, consists of hexagonal arrangements of Si–O–Si units. In the model oxygen atoms saturate all silicon atoms at the pore surface. Oxygen atoms with less than two silicon atoms attached to them are saturated by hydrogen atoms. All hydroxyl groups are located at the outer surface.

That way, the pore diameter of 0.9 nm of the model constructed in a previous study [21] was increased up to 5.5 nm. From this 2D layer structure the 3D structure was generated by using the built module on the Hyperchem 8.01 software (Hypercube, Inc. Gainesville, FL). Successive layers were added until 3.71 nm length. The final 3D structure was refined by optimization of the geometry using the 500 steps of Steepest-Descent and 1500 steps Polak-Ribiere conjugate gradient algorithms both using the MM+ force field, mainly developed for organic molecules as an extension of MM2 force field. The minimization process concluded when the energy converged or until a gradient of 0.1 kcal/mol. Because the big size of SBA-15 a molecular orbital study was not be performed. Nevertheless in a previous paper [21] with a smaller molecule and from its refined geometry, a semiempirical molecular orbital method using the AM1 algorithm, allowed us to obtain the total energy of the system, the atom charge distribution and the electrostatic potential of the molecule. These results can be extrapolated to the model proposed in the present study.

Similarly, the same sequence of calculations was performed for the CSB as well as the structure of SBA-15 functionalized with APTES chains. The crystalline structure of CSB molecule was obtained from the PDB link [32] and different conformations were calculated by molecular dynamics assays. Molecular dynamic of duration 10 ps was performed and the conformers were collected. The structure is sufficiently rigid so the molecular dynamics gave no notable energy differences between different conformations.

On the other hand, another model was constructed considering a different interaction in which the amino groups were not free towards the interior or outside of the surface, but that has been considered that they were adsorbed by charges interaction on the surface. This way the $–NH_2$ groups are united to the free –OH groups that are to an interaction distance and considering positive charge on the nitrogen atom i.e. $– NH_3$. Later on, a minimization of the energy was carried out by using the Steepest-Descent and Fletcher-Reeves algorithms until a convergence value in this case of 0.5 kcal/mol.

The CSB docking on the surface of SBA–15 and SBA15-APTES was carried out by using the Argus Lab software (ArgusLab 4.0.1 Seattle, WA Planaria Software LLC) in a computer-assisted molecular modelling, which uses either AScore or the Lamarckian genetic algorithm, scoring functions to find the low-energy binding modes [33]. These results were then verified and corroborated with the program Autodock 4.0. The binding site was again defined from the coordinates of the ligand (CSB) in the SBA-15 and SBA15-APTES 3D theoretical models. Argusdock exhaustive search docking engine was used [33,34], with grid resolution of 0.040 nm. Docking precision was set to ‘high precision’ and ‘flexible ligand docking’ mode was employed for each docking run. These calculations used a cubic box of 3.83 nm x 5.68 nm x 5.32 nm. To determine the interaction of CSB with the solvent, a docking experiment was carried out. Calculations were made with approximately 800 water molecules inside the matrix.

## 3. Results and discussion

### *3.1 Matrixes characterization before and after the functionalization*

Small-angle XRD of SBA-15 (Fig.1) shows a well resolved 2D-hexagonal pattern with (10), (11) and (20) reflections for both SBA-15 and SBA15-APTES [35]. The values for the spacing of d10 reflection were: SBA-15, 10.25 nm (average $a_o$= 11.83 Å) and SBA-15-APTES, 10.16 (average $a_o$= 11.73 Å). Calculated pore wall thicknesses were: SBA-15, 11.83 Å ($a_o$) – 10.1($D_P$)=1.73 nm and SBA-15-APTES:

11.73 Å ($a_o$) –8.6 ($D_P$)=3.13 nm. Pore diameters (see Table I) decrease after CSB adsorption in SBA-15 and SBA15-APTES (1.2 nm and 3.6 nm respectively).

The similarity between both XRD patterns evidences that the functionalization of the matrix pore walls does not affect significantly the structural order. This minimum variation observed was already reported for analogous systems with APTES functionalization degrees of the nominal total amount of Si–OH on material surface as high as 75% or 100% [36]. Consequently a functionalization of 20% as performed in the present study must lead to a XRD pattern virtually identical to that of the native SBA-15 as it can be observed in Fig. 1.

On the other hand, CHN elemental analysis of SBA-15-APTES reveals the presence of carbon (7.3 wt-%) and nitrogen (2.2 wt-%), which corresponds to a content of functional groups of 1.6 meq/g, which fairly agrees with the theoretical value that must be obtained in the experimental conditions performed. FTIR analysis of SBA-15 treated with APTES (results not-shown) confirmed that SBA-15 surface was effectively grafted with aminopropyl moieties in the SBA-15-APTES sample.

In a previous paper of our research group, NMR and FTIR analyses clearly showed SBA-15 functionalization. Besides, the pores were not blocked in this case [37].

*3.2 Textural properties: pore diameter, pore volume, surface area*

Nitrogen isotherms and pore size distribution of SBA-15 and SBA15-APTES materials are shown in Fig. 2. Table I summarizes the most relevant values obtained from the isotherms. The adsorption isotherms show a sharp increase of the amount of nitrogen adsorbed at $P/P_0$ <0.6-0.8, corresponding to the capillary condensation of nitrogen inside the pores. Another remarkable characteristic is the hysteresis loop of the isotherms, corresponding to type IV isotherms with type H1 hysteresis, which are characteristics of cylindrical pores open at both ends [38]. As expected, coating the pore surface with aminopropyl moieties leads to a decrease in pore diameter, surface area and pore volume. As it is observed, native SBA-15 exhibited a very narrow pore size distribution. However, after the functionalization with APTES a substantial decrease in the pore size diameter (Table I) together a slight increase in the pore size distribution (Figure 2B) was observed.

*3.3 CSB absorption*

Both SBA-15 based materials developed an intense blue colour after contacting with the CSB solution, which is a first indication on the successful absorption of the biomolecule in the matrixes. Furthermore, characteristic IR bands of this molecule at 1413 and 665 $cm^{-1}$ were observed in the FTIR spectra of loaded samples (data not shown). Elemental and TG analyses indicate that the total amount of CSB adsorbed was 14 wt-% in the SBA-15 matrix and 16 wt-% in the functionalized one. These small differences between both matrixes could be explained considering the great size of the pores compared with the pore decrease observed after functionalization. The XRD of the samples after CSB adsorption did not showed a lost of structural ordering.

On the other hand, the nitrogen adsorption isotherms of CSB containing samples revealed noticeable changes as compared with the original matrixes. That way, surface area, pore volume and average pore diameter decreased after the biomolecule adsorption. In the unmodified SBA-15, a shift of the average pore size from 10.1 to 8.9 nm was observed, while in the functionalized sample the pore size decreased from 8.6 to 5.0 nm (Table I). However, the hysteresis loop corresponding to the pore filling by nitrogen is still present in the isotherms, which shows that the CSB molecules packed inside the channels do not fully occupy all the available space. This result suggests that the CSB molecules are packed forming a layer on the pore wall. The differences between the native and the functionalized matrixes in regards to the observed reduction of pore size after drug loading might result from differences in the orientation of the adsorbed molecules respect to the pore surface. Also remarkable was the presence of microporosity in the SBA-15 sample, a feature of this structure [39], whereas no microporosity was found in the samples containing CSB. All these facts prove the presence of the biomolecule inside the pores after the adsorption process.

*3.4 CSB delivery: HPLC measurements*

Fig. 3 shows the percentage of CSB released with time after soaking SBA-15 and SBA-15-APTES materials in SBF solution. In this figure each measurement were performed in triplicate and the standard deviation was calculated. These results indicate that the delivery process from SBA-15 is extremely fast (A trace) compared with the previously reported results on the delivery of ibuprofen, erythromycin and gentamicin [20,40] as well as with SBA-15-APTES (B trace). This fact that could be initially explained taking into account the strong interactions of the four sulphonic groups of CSB (partially ionized at physiological pH) with the solvent and the matrix, are analyzed later by molecular modelling.

In comparison, the functionalized sample evidence a much lower delivery rate, while an almost complete release of the colorant is observed after 72 h. This result proves the effective influence of the functionalization in the delivery process, achieving the purpose of controlling the CSB release rate.

For these delivery processes, the diffusion model used considers the leaching of the colorant by the bathing fluid, which is able to enter in the molecule-matrix interface through the macropores. CSB is presumed that is not introduced in the micropores and we did not consider that effect.

To calculate the observed constant *k*, the amount of CSB released was plotted versus the square root of time using linear regression according with the Higuchi model [41]. The kinetic constant obtained for SBA-15 native was 34.7 $min^{-1/2}$, being the correlation factor of 0.99. This result confirms that the release kinetics adjusts to the Higuchi model.

On the other hand, for SBA-15-APTES, the kinetic constant obtained was 7.7 $h^{-1/2}$ by applying the Higuchi model, being the correlation factor 0.96.

From the obtained kinetic constants it can be clearly appreciated that the release of CSB in SBA-15-APTES is much slower and maintained with respect to the native SBA-15, approximately two orders of magnitude. Thus, in the case of the non-functionalized matrix, 100% of the drug it is released in 4.5 minutes approximately, whereas for the functionalized matrix, this happens in 72 hours (See Fig. 3). These results could be expected but they are much more intense that in other studied drug models [42]. To investigate these results, a molecular model of SBA-15 before and after be chemically modified with APTES was constructed.

*3.5 Molecular modelling and docking calculations*

As it can be observed in Figure 4, CSB consists of very polar, symmetric and rigid molecule of 2.74 nm x 1.11 nm in size. Previously to the molecular dynamics calculations, molecular orbital studies and molecular mechanics were carried out. The dynamics studies confirmed the rigidity of the molecule and in Fig. 4 the most probable conformation for this molecule is shown. The dimensions of the molecule are compatible with the size of the SBA-15 matrix.

To approximate the calculations to the real system, negative charges were assigned to the four sulphonate groups R–$SO_3H$ of CSB, so that the interaction with matrix was carried out of in a more effective way. These charges were obtained by molecular orbital (MO) calculations on the colorant molecule. The pKa of the sulphonic groups are -3.3, -2.8, -2.4 and -2.0, respectively and for this reason they are totally ionized to R–$SO_3^-$. These values were obtained from the charge density on every atom in the molecule obtained by using *ab initio* methods with the 6-31G* algorithm (calculations not shown). From these results can be deduced that is a strongly acidic molecule. It must take into account that although in the vacuum the molecule is not ionized, the modelling calculations were carried out but following this negative charge assignation.

Moreover, it was possible to obtain the electrostatic potential of CSB, as observed in Figure 5. The figure shows that the electrostatic potential of CSB is essentially negative. However the silica matrix has an essentially positive electrostatic potential. [21] For this reason, the CSB molecule can penetrate into the matrix channels and interact with the silica surface through the sulphonic groups.

On the other hand, a mesoporous silica matrix model with pore diameter of 5.45 nm and a length of 3.7 nm long was built for the first time. Thus, CSB molecules would be able to penetrate by size into the matrix channels, as depicted in Figure 6A, and also in the channels of the functionalized matrix with APETES chains used for the docking calculations (Fig. 6B). Fig. 6C displays a magnification of Fig. 6B in which the interaction of the CSB molecule with the functionalized surface of the matrix is visualized with more detail. The study by docking showed that CSB molecule penetrates inside of the tube in both cases as it is shown in Fig 6.

Since the adsorption and release of CSB take place in aqueous media we also made the docking calculations using water as solvent to simulate the explicit dielectric constant of media, as it was described in the materials and methods section. The experiment was carried out considering water molecules like as the union sites (Figure 7) and interaction energy obtained was –5.27 Kcal/mol. The difference of this value and the energy of interaction of CSB with non functionalized matrix is close to 1 Kcal/mol. As it was expected, these results indicate the greater preference of CSB molecule by the solvent because the higher polarity of water and CSB molecules compared with the silica matrix. Therefore, these calculations did not yield differences between functionalized and non functionalized matrixes with respect to their behavior with the water. For this reason, to simplify the process, all calculations presented in this study were made in vacuum.

Docking calculations between CSB with non functionalized SBA-15 (Fig. 6A) gave an energy interaction with the inner part of pores of -4.37 Kcal/mol. On the other hand, the interaction with the external surface was something smaller: -3.93 Kcal/ mol (Fig. 6A). Given the high specific surface area of these materials, the proportion of molecules in the inner part is far beyond those that could be placed in the external surface reason why we can assume that the interaction is made of this way. However OH groups are distributed towards the interior and the outside of the channel. When the experiment of docking is performed with the surface functionalized with APTES molecules, the value of the interaction energy is something smaller, -4.21 Kcal/mol (Fig. 6B). When the interaction of the molecule with the functionalized matrix was carried out on the external surface of the model, the interaction energy obtained was -3.91 Kcal/mol. These results suggest that interaction on the surface when is functionalized or not, is of the same order of magnitude, since it was not considered a functionalization in the outer part of the matrix to obtain a model as simple as possible.

If we use the studied system like a system of prediction of drug liberation, where we are playing with the polarities of the drug, the matrix surface, and the solvent and since the solvent in the organism cannot be modified, the only variables possible to modify would be the substrate and the surface functionalization. If we want to study how the liberation of a certain drug would take place, a previous study would have to be made *in silico* as previous step to the *in vivo* study in determining what kind of functionalization is better adapted to guarantee the more adequate kinetic of release.

From the results shown it can be deduced that the functionalization does not explain neither the slower kinetic of release that take place in the case of the functionalized matrix nor the reduction of pore diameter experimentally observed (see Table 1) reason why only an interaction of the propyl amino groups with the matrix surface could explain these facts. In this sense Li and col described three possible interactions of the amino propyl groups on the surface of a silica matrix [43].

It must be take into account that SBA-15 contains Si–OH groups in a proportion of 1/5 $Q^3$ and 4/5 $Q^4$ with pKa ≈ 2 and ≈ 8.2, respectively [44]. Moreover SBA-15-APTES, that containing $R–NH_2$ amino groups with pKa ≈ 9.6 as is well known. At the pH of 7.4 at which our kinetic experiment was performed, the silanol groups are in a neutral form of Si–OH or ionized $Si–O^-$ whereas the amino groups are ionized as $R–NH_3^+$ (approximately 95-99%).

In a previous paper, $^{29}Si$ NMR analyses were performed to determine the population of silanol groups. It clearly showed a decrease $Q^2$ and $Q^3$ percentage, as well as a remarkable increase in $Q^4$ signal, when functionalized with APTES (post-synthesis) [45].

In agreement with the model proposed by Li et al [43], the amino propyl groups could remain towards the inner or the outer part of the matrix. Moreover internal dual ions could be formed towards the interior or the outer part in which free –OH groups would also form hydrogen bonds with amino $–NH_2$ groups and these groups could be adsorbed directly on the matrix surface by charge interactions. See Fig. 8A. Only this interaction could result in a deformation of the matrix that could diminish the pore size, which would be transcendental to slow down the CSB release from functionalized matrix compared with native SBA-15. This hypothesis would be compatible with the functionalization model proposed.

Bearing in mind this possibility, we made an *in silico* experiment considering that takes place an interaction by hydrogen bond between the free –OH and amino $NH_2$ groups (see section 2.3). In the figure 8B this interaction is also outlined that supposes a tube deformation as well as a remarkable pore size reduction, which is in agreement with the results of the absorption-desorption isotherms. In the figure two models obtained by molecular mechanics calculations are superimposed clearly evidencing the substantial contraction experimented for the SBA-15 matrix after the functionalization with APTES when the interaction with the matrix is considered. In this simulation aminopropyl groups interact with the matrix and hence subsequent channel deformation takes place; the aminopropyl groups are randomly oriented both inside and outside the matrix.

The interaction of CSB with the matrix functionalized by this procedure evaluated by docking did not diminish significantly the energy of interaction with the matrix (–4.25 *vs* –4.21 Kcal/mol). For this reason we can conclude that the APTES functionalization does not significantly favor a greater interaction with the CSB molecule. Therefore is the pore size decrease the factor, which more contributes to the greater retention in the surface of the functionalized matrix with respect non functionalized and would explain the considerably slower kinetic of release. These facts are described for the first time contributing a new vision on this process of functionalization.

## 4. Conclusions

The molecular model of SBA-15 built for the first time explains the differences in the release kinetics of CSB from SBA-15 matrixes, which decreased two orders of magnitude after functionalizing with 3-aminopropyl-triethoxy-silane, APTES. The model showed that, although electrostatic interactions drug-matrix takes place, the key factor is the distortion of the matrix produced by the interaction of the amino groups of APTES originating a decrease in the pore size. This effect not previously reported for other chemical modifications justify the higher retention of CSB in SBA-15-APTES compared with native SBA-15.

***ACKNOWLEDGEMENTS***

Financial support thought Comisión Interministerial de Ciencia y Tecnología (CICYT, Spain) (MAT2012-35556), Comunidad Autónoma de Madrid (S2009/MAT-1472) and the Network of Excellence of Spanish MICINN (CSO2010-11384-E) is acknowledged. I. Galan is acknowledged for the work performed in her final of master project.

## REFERENCES

1. A. Rimola, D. Costa, M. Sodupe, J.-F. Lambert, P. Ugliengo, Chem. Rev. 113 (2013) 4216−4313.
2. G. Gronau, S.T. Krishnaji, M. E. Kinahan, T. Giesa, J.Y. Wong, D.L. Kaplan, M.J. Buehler, Biomaterials 33 (2012) 8240–8255.

3. N. Haddish-Berhane, J.L. Rickus, K. Haghighi, Int J Nanomedicine 2 (2007): 315–331.
4. N. Foloppe, R. Hubbard, Curr. Med. Chem. 13 (2006) 3583–3608.
5. N.H. de Leeuw, Z.M. Du, J. Li, S. Yip, T. Zhu, Nano Lett. 3 (2003) 1347–1352.
6. M. Delle Piane, M. Corno, P. Ugliengo, J. Chem. Theory Comput. 9 (2013) 2404−2415.
7. M. Vallet-Regi, ISRN Mater. Sci. (2012) pp not given. (20 pages) Article ID 608548.
8. M. Manzano, M. Vallet-Regi, Prog. Solid State Chem. 40 (2012) 17–30.
9. M. Manzano, M. Colilla, M. Vallet-Regi, Expert Opin. Drug Deliv. 6 (2009) 1383–1400.
10. M. Vallet-Regi, F. Balas, D. Arcos, Angew. Chem. Int. Ed. 46 (2007) 7548–7558.
11. T. Yanagisawa, T. Shimizu, K. Kuroda, and C. Kato, Bull. Chem. Soc. Jpn., 63, (1990) 988–992.
12. C. T. Kresge, M.E. Leonowicz, W. J. Roth, J. C. Vartuli, J. S. Beck. Nature 359 (1992) 710–712.
13. S. Inagaki, Y. Fukushima, K. Kuroda**,** J. Chem. Soc., Chem. Commun. 8 (1993) 680–682.
14. S. Inagaki, S. Guan, T. Ohsuna, O. Terasaki, Nature, 416, (2002). 304–307.
15. S. Che, Z. Liu, T. Ohsuna, K. Sakamoto, O. Terasaki, T. Tatsumi, *Nature*, 429 (2004). 281–284.
16. M. Vallet-Regí, A. Ramila, R.P. del Real, J. Perez-Pariente, Chem. Mater 13 (2001) 308–311.
17. B. Muñoz, A. Ramila, J. Perez-Pariente, I. Diaz, M. Vallet-Regí. Chem. Mater. 15 (2003) 500–503.
18. F. Bai, O.A. Asojo, P. Cirillo, M. Ciustea, M. Ledizet, P.A. Aristoff, L. Leng, R.A. Koski, T.J. Powell, R. Bucala, K.G. Anthony. J Biol Chem. 31 (2012) 30653-63.
19. E. Lima, J. Flores, A.S. Cruz, G. Leyva-Gómez, E. Krötzsch. Microporous and Mesoporous Materials. 181 (2013) 1-7.

20. A.L. Doadrio, E.M.B. Sousa, J.C. Doadrio, J. Pérez-Pariente, I. Izquierdo-Barba, M. Vallet-Regí, J. Control. Release 97 (2004) 125–132.

21. A.L. Doadrio, J.C. Doadrio, J.M. Sánchez-Montero, A.J. Salinas, M. Vallet-Regi, Micropor. Mesopor. Mat. 132 (2010) 559–566.

22. S. Roseth, E. M. Fykse, F. Fonnum, J. Neurochem. 65 (1995) 96–103.

23. A. Beirith, A. R. S. Santos, J. B. Calixto. Brain Res. 924 (2002) 219–228.

24. D. J. Clanton, R.A. Moran, J. B. McMahon O. S. Weislow, R. W. Buckheit, M. G. Hollingshead, V. Ciminale, B. K. Felber, C. N. Pavlakis, J. P. Bader. J Acquir. Immune Defic. Syndr. Hum. Retrovirol. 5 (1992) 771–781.

25. A. Pal, B.K. Mishra, S, Panigrahi, R.K. Nath, S. Deb. J. Macromol. Sci. Part A-Pure Appl. Chem. 48 (2011) 619–624.

26. N. Sueyoshia, T. Takaoa, T. Nimuraa, Y. Sugiyamaa, T. Numanoa, Y. Shigerib, T. Taniguchic, I. Kameshitaa, A. Ishida, Biochem. Biophys. Res. Commun. 23 (2007) 715–721.

27. D. Zhao, Q. Huo, J. Fena, B. F. Chmelka and G. D. Stucky. J. Amer. Chem. Soc. 129 (1998) 6024–6036.

28. T. Kokubo, H. Takadama. Biomaterials 27 (2006) 2907–15.

29. E.P. Barrett, L.G. Joyner, P.P. Halenda, J. Am. Chem. Soc. 73 (1951) 373–380.

30. M. Kruk, M. Jaroniec, A. Sarayi. Langmuir. 13 (1997) 6267-6273.

31. http://www.chm.bris.ac.uk/motm/mcm41/mcm41.htm

32. **DOI:**10.2210/pdb3u18/pdb.

33. G. M. Morris, D. S. Goodsell, R.S. Halliday, R. Huey, W. E. Hart, R. K Belew, A. J. Olson, J. Comput. Chem. 19 (1998) 1639-1662.

34. G.M. Morris, R. Huey, W. Lindstrom, M.F. Sanner, R.K. Belew, D.S. Goodsell, A.J. Olson, J. Comput. Chem. 30 (2009) 2785–2791.

35. D. Zhao, J. P. Feng, Q. S. Huo, N. Melosh, G. H. Fedrickson, B. F. Chemelka, G.D. Stucky, Science 279 (1998) 548–552.
36. A. Nieto F. Balas, M. Colilla, M. Manzano, M. Vallet-Regi. Micropor Mesopor Mater 116 (2008) 4–13.
37. M. Colilla, I. Izquierdo-Barba, S. Sánchez-Salcedo, J.L. G. Fierro, J. L. Hueso, M. Vallet-Reg. Chem. Mater. 22 (2010) 6459–6466.
38. S. Che, K. Lund, T. Tatsumi, S. Iijima, S. H. Joo, R. Ryoo, O. Terasaki. Angew. Chem. Int. Ed. 42 (2003) 2182–2185.
39. A. Galarneau, H. Cambon, F. Di Renzo, R. Ryoo, M. Choi, F. Fajula. New J. Chem. 27 (2003) 73–79.
40. M. Vallet-Regí, J. C. Doadrio, A.L. Doadrio, I. Izquierdo-Barba, J. Pérez-Pariente. Solid State Ionics 172 (2004) 435–439.
41. T. Higuchi,. J. Pharm. Sci. 52 (1963) 1145–1147.
42. M. Vallet-Regi, E. Ruiz-Hernandez, Adv. Mater, 23 (2011) 5177–5218.
43. Y. Li, B. Han, L. Liu, F. Zhang, L. Zhang, S. Wen, Y. Lu, H. Yang, J. Shen. Compos. Sci. Technol. 88 (2013) 69–75.
44. J. M. Rosenholm JM Czuryszkiewicz T, Kleitz F, Rosenholm JB, Lindén M, Langmuir 23 (2007) 4315–4323.
45. B. Gonzalez, M. Colilla, C. López de Laorden M. Vallet-Regí. J. Mater. Chem. 19 (2009), 9012–9024.

## Figure Captions

**Fig. 1.** Low angle XRD patterns of native SBA-15 and SBA-15-APTES materials.

**Fig. 2.** $N_2$ adsorption isotherms and pore size distributions of: (A) SBA-15 before and after CSB adsorption, and (B) SBA15-APTES before and after CSB adsorption.

**Fig. 3.** CSB release profiles from (A) SBA-15 and (B) SBA15-APTES. Note the different scales of time: minutes in (A) and hours in (B).

**Fig. 4.** CSB molecular structure and geometrical dimensions.

**Fig. 5.** CSB molecule electrostatic potential.

**Fig. 6**. (A) CSB-loaded SBA-15 (in vacuum), (B) CSB loaded SBA15-APTES (in vacuum) (C) A magnification of B showing the interactions of CSB with SBA-15 matrix and APTES molecules.

**Fig. 7.** The interaction energy of CSB with water molecules –5.27 Kcal/mol is superior to the interaction with the matrix –4.37 Kcal/mol.

**Fig. 8.** (A) Schematic representation of different types of interaction of APTES and SBA-15 and (B) Superimposed functionalized matrixes with amino chains directed towards the interior of the pores and considering as well a direct interaction of the amino groups with the silica matrix.

Figure 1
Click here to download high resolution image

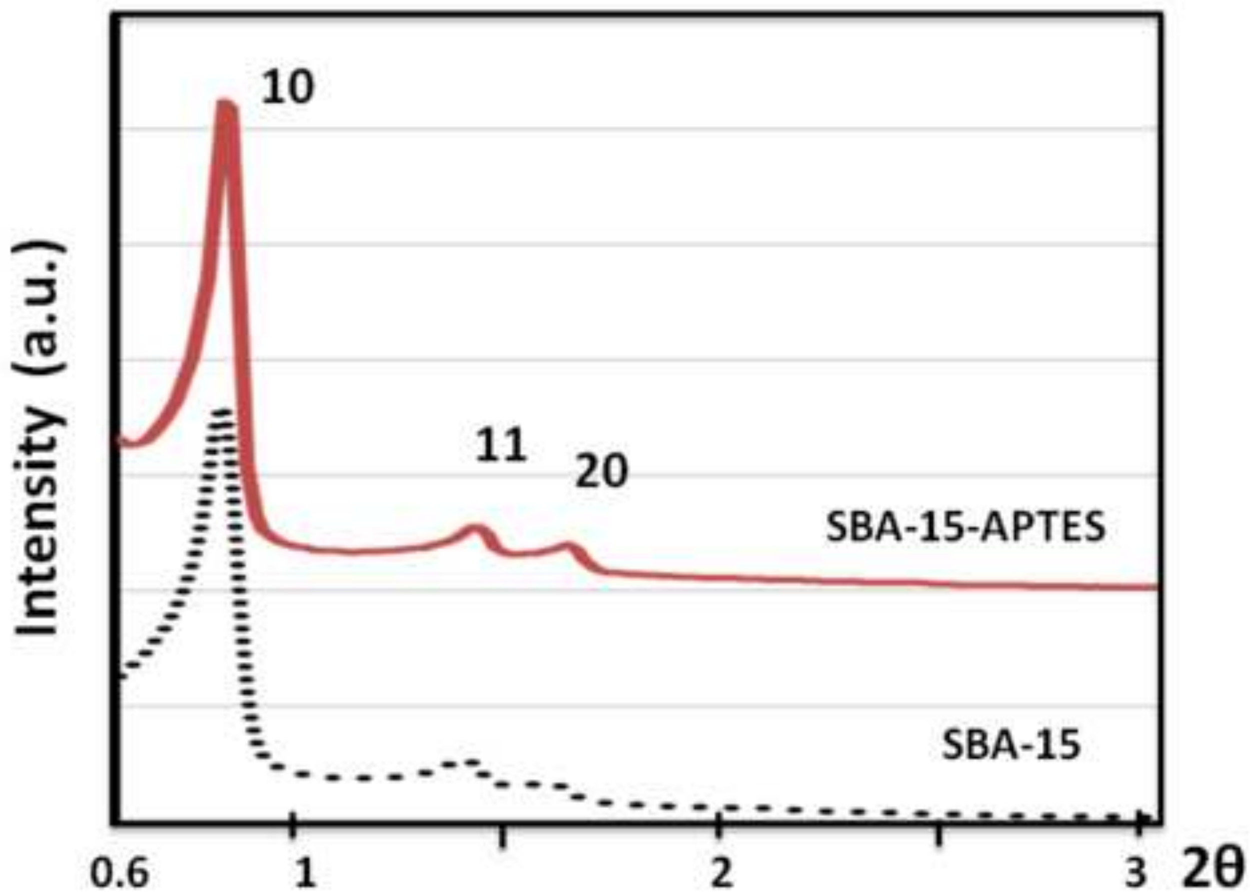

Figure 5
Click here to download high resolution image

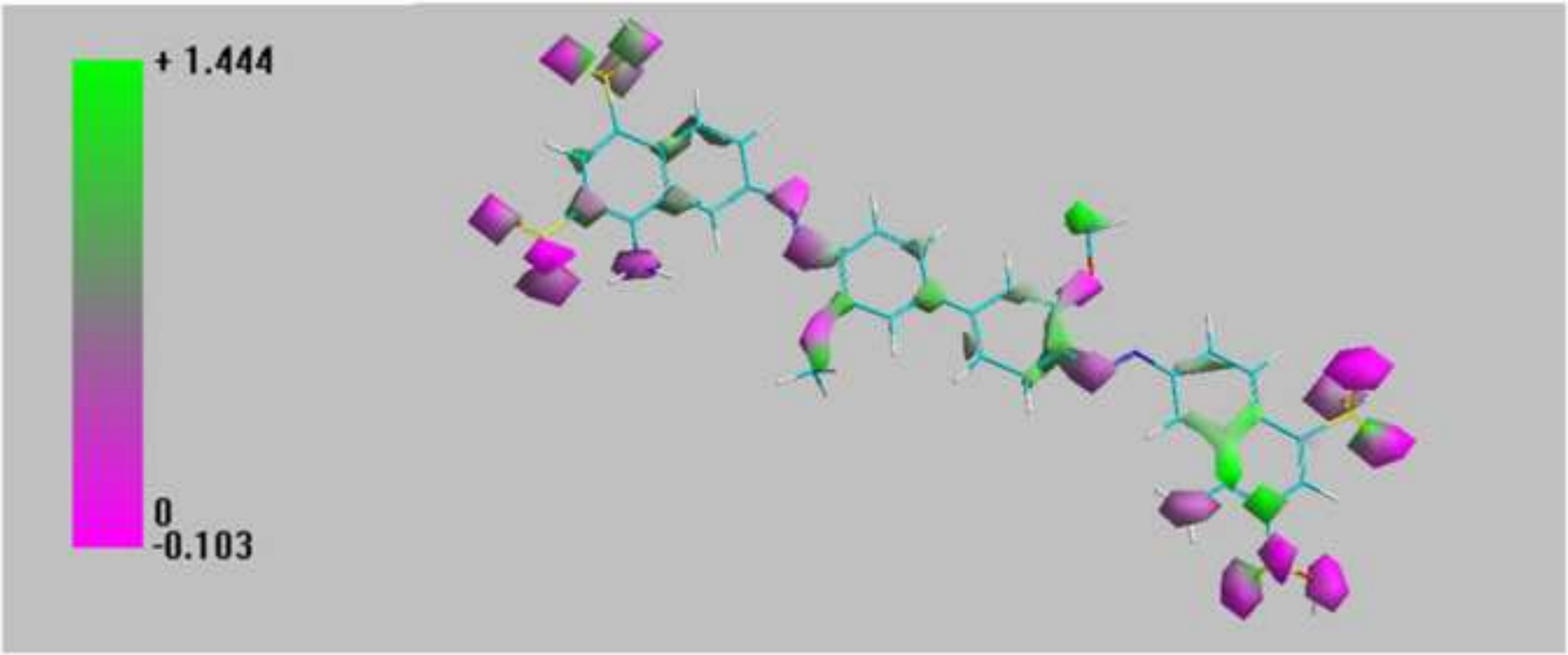

Figure 7
Click here to download high resolution image

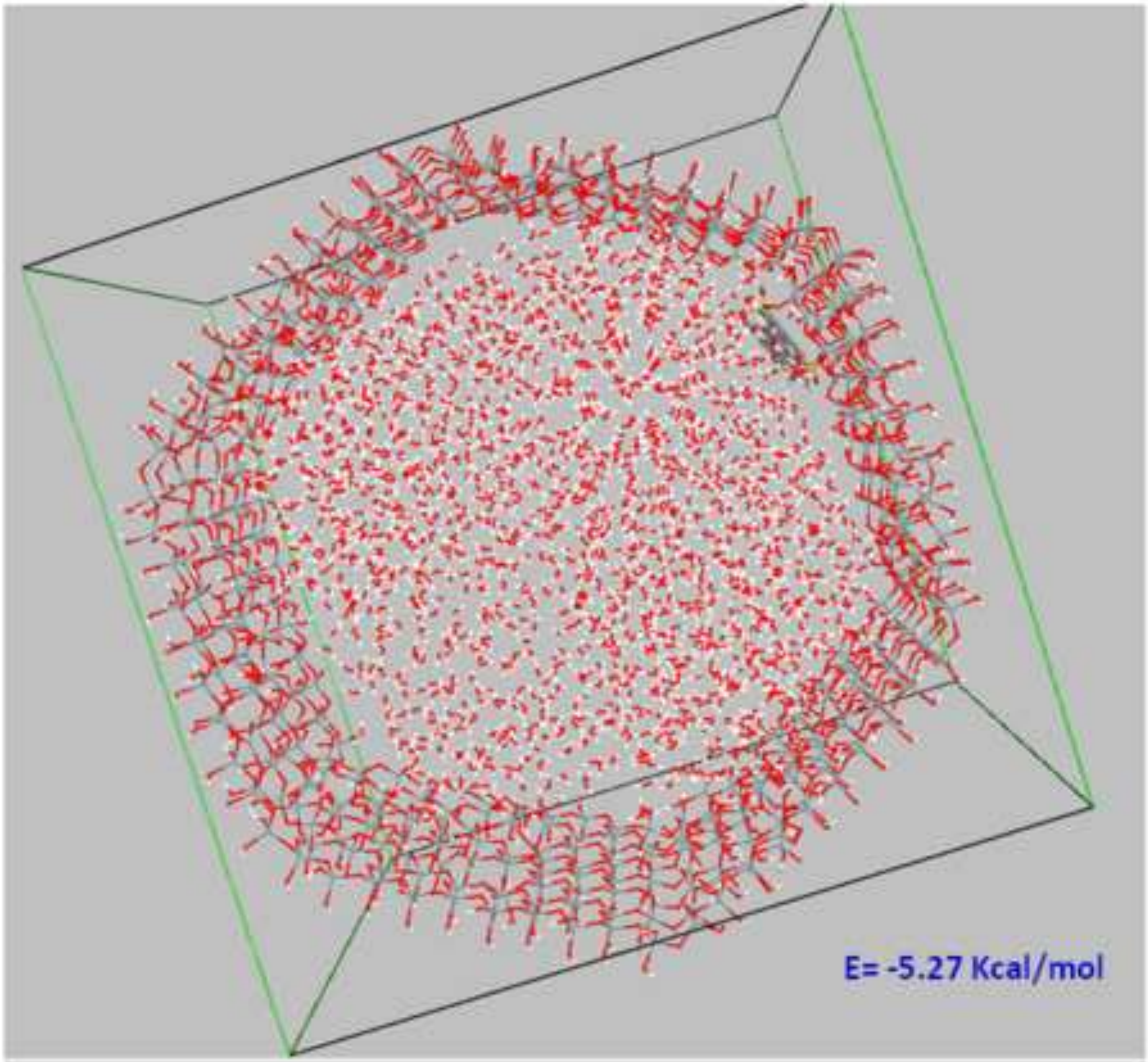

Figure 2
Click here to download high resolution image

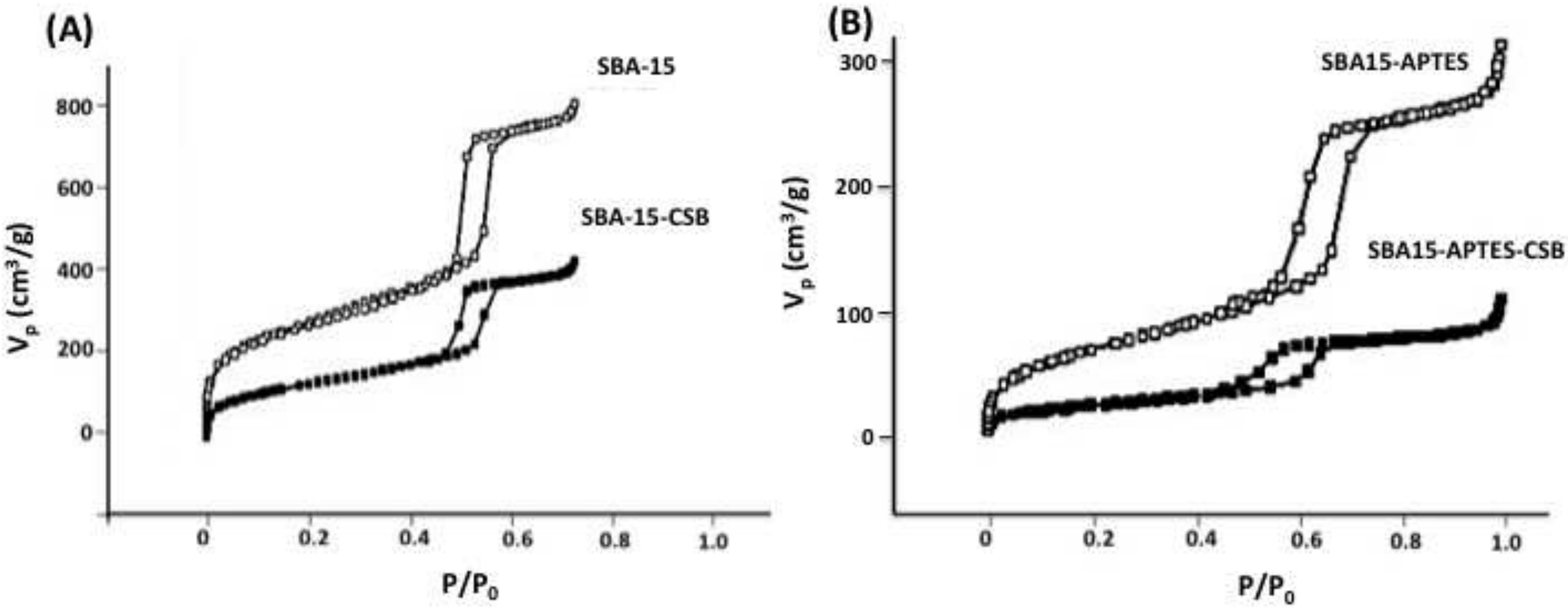

Figure 3
Click here to download high resolution image

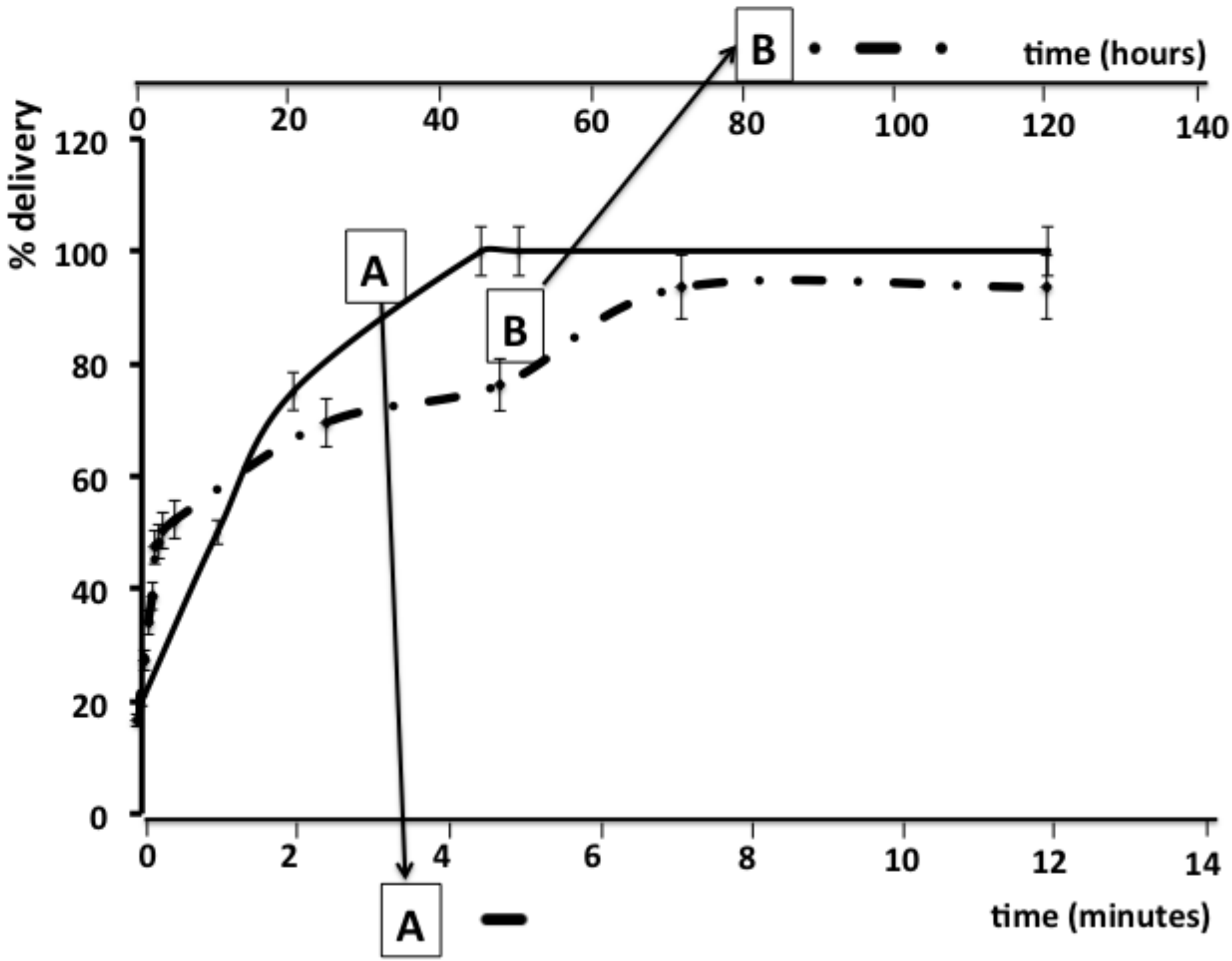

Figure 4
Click here to download high resolution image

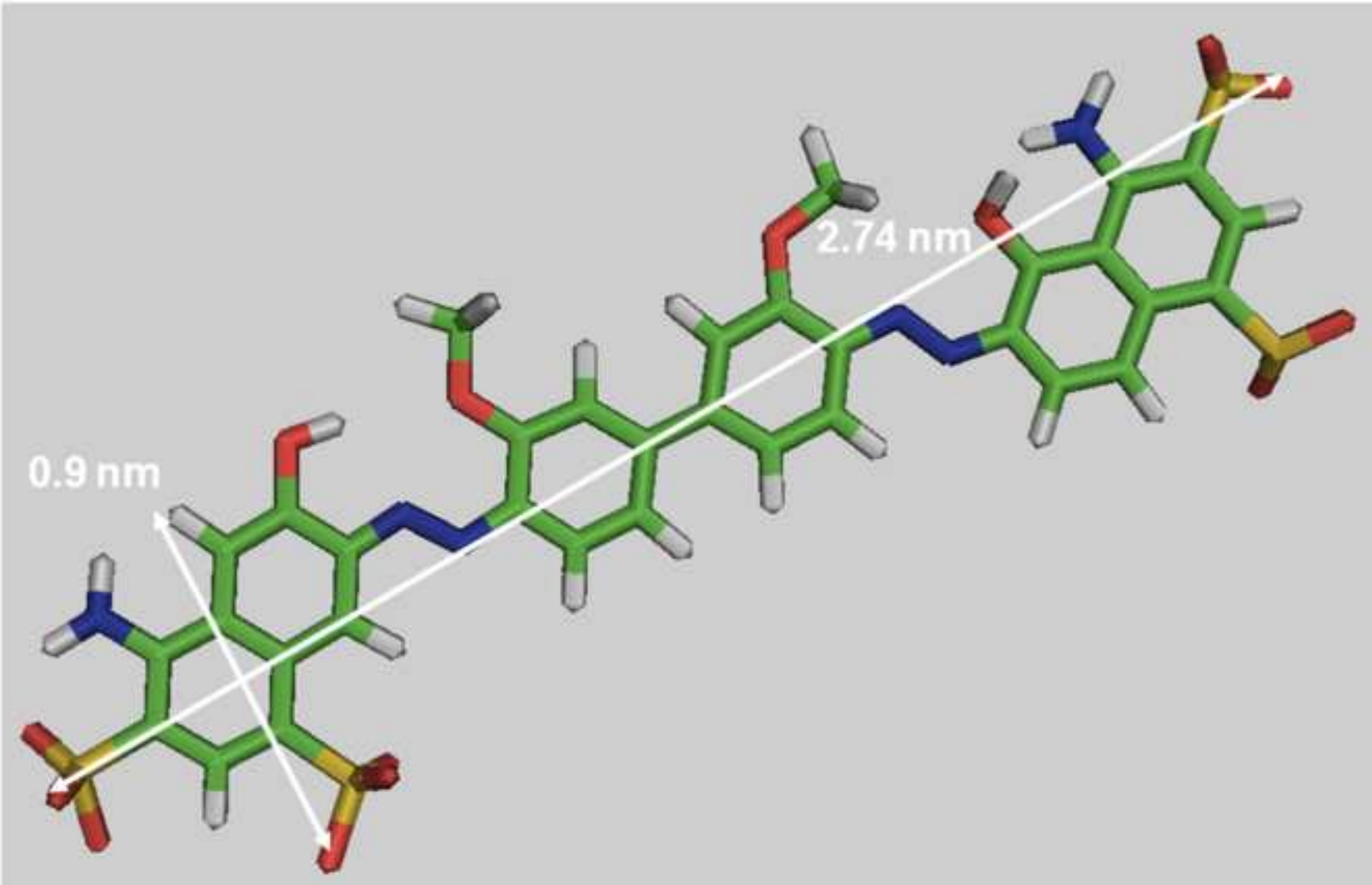

**Figure 6**

**Click here to download high resolution image**

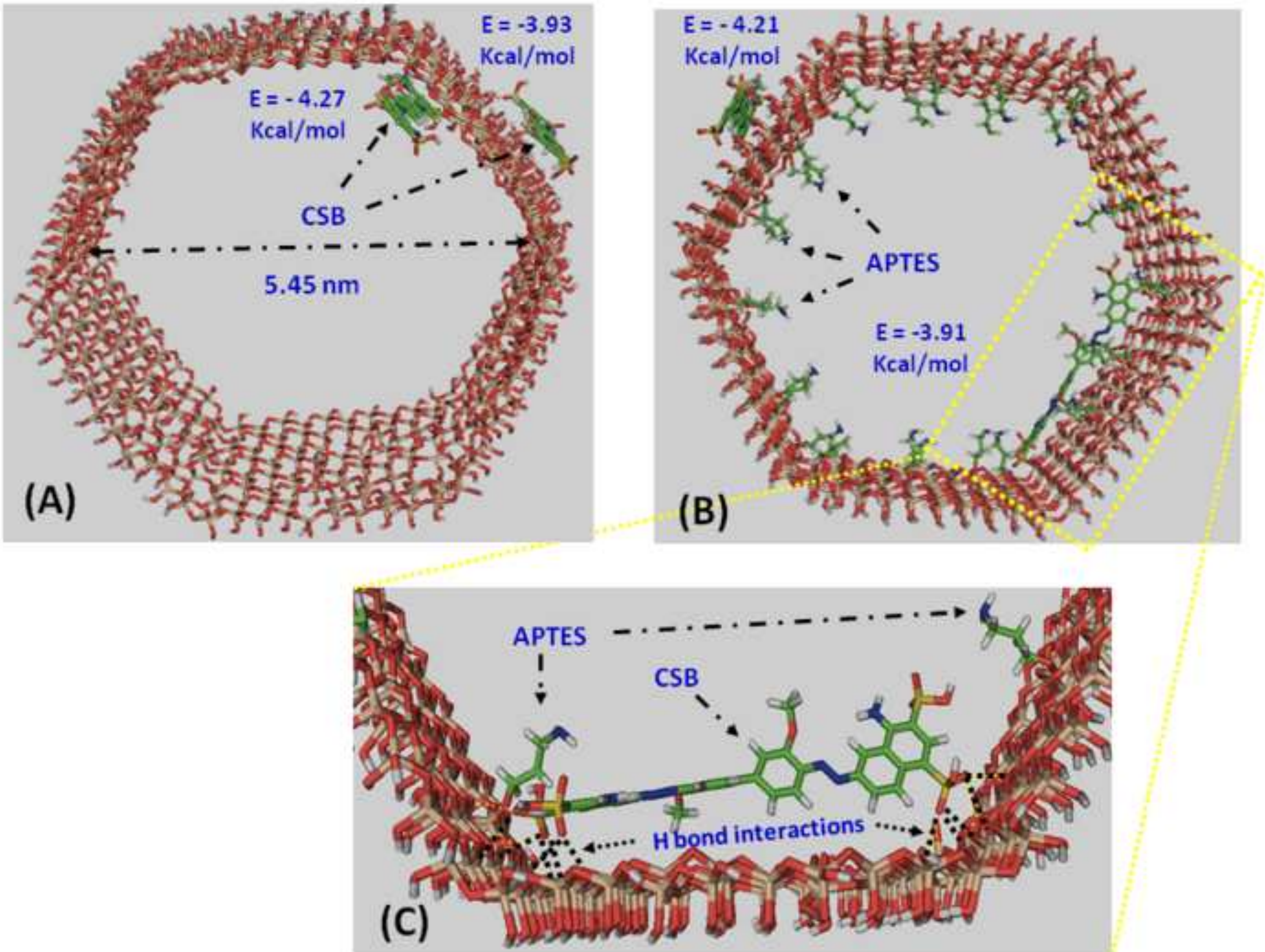

**Figure 8**

Click here to download high resolution image

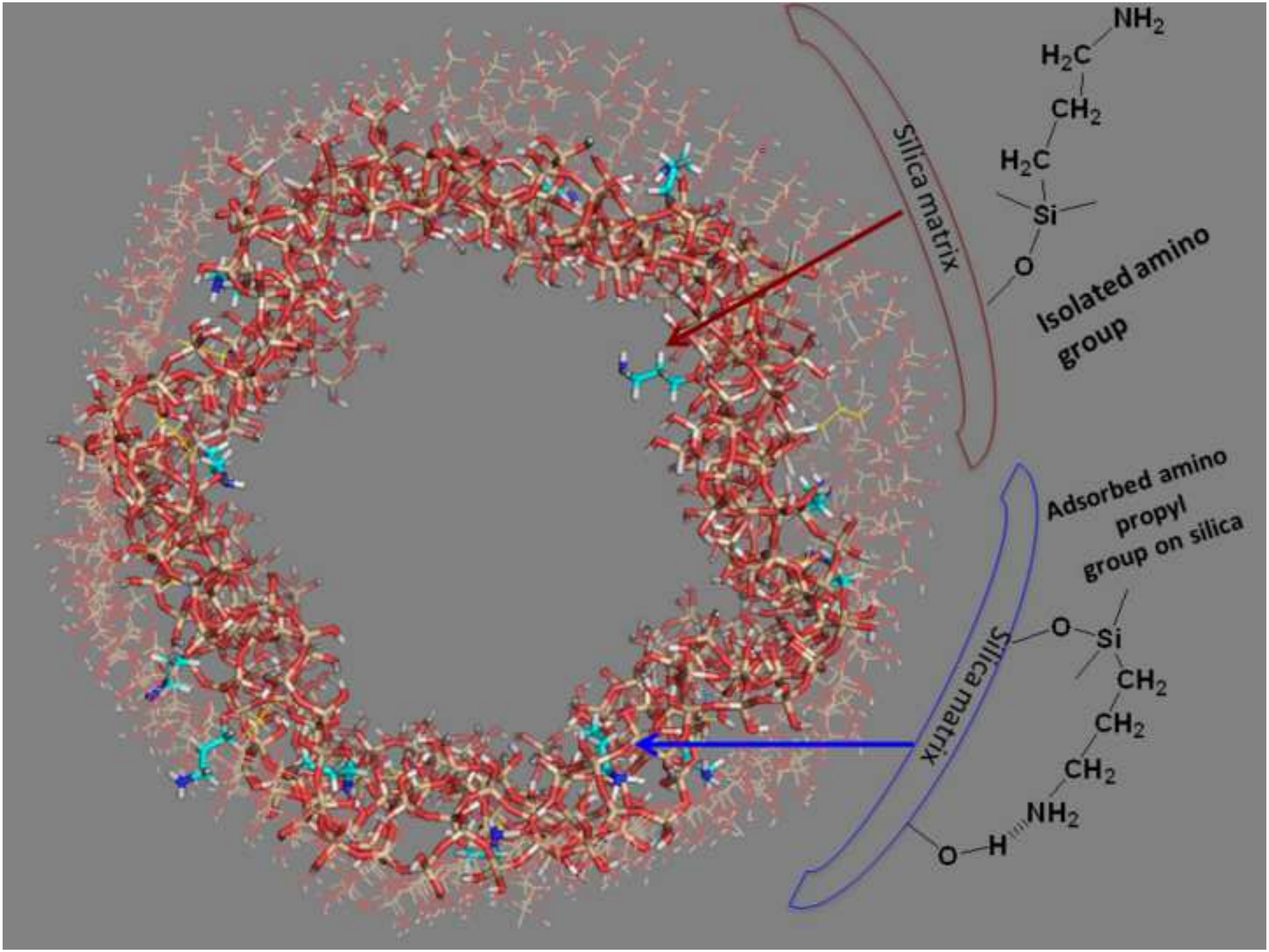

**Table I**

**Table I**. Textural properties of the samples obtained from $N_2$ adsorption measurements.

| Sample | $S_{BET}$ ($m^2/g$) | $V_P$ ($cm^3/g$) | $V_{\mu P}$ ($cm^3/g$) | D (nm) |
|---|---|---|---|---|
| SBA15 | 920 | 1.234 | 0.555 | 10.1 |
| SBA15-CSB | 435 | 0.654 | - | 8.9 |
| SBA15-APTES | 260 | 0.496 | - | 8.6 |
| SBA15-APTES-CSB | 89 | 0.174 | - | 5.0 |